



OPEN

The hybrid lattice of $K_xFe_{2-y}Se_2$: where superconductivity and magnetism coexist

SUBJECT AREAS:

SUPERCONDUCTING
PROPERTIES AND
MATERIALSELECTRONIC PROPERTIES AND
MATERIALSMAGNETIC PROPERTIES AND
MATERIALSPHASE TRANSITIONS AND
CRITICAL PHENOMENADespina Louca¹, Keeseong Park^{1*}, Bing Li¹, Joerg Neuefeind² & Jiaqiang Yan^{2,3}¹Department of Physics, University of Virginia, Charlottesville, VA 22904, USA, ²Oak Ridge National Laboratory, Oak Ridge, TN 37831, USA, ³Department of Materials Science and Engineering, The University of Tennessee, Knoxville, TN 37996, USA.

Much remains unknown of the microscopic origin of superconductivity in atomically disordered systems of amorphous alloys or in crystals riddled with defects. A manifestation of this conundrum is envisaged in the highly defective superconductor of $K_xFe_{2-y}Se_2$. How can superconductivity survive under such crude conditions that call for strong electron localization? Here, we show that the Fe sublattice is locally distorted and accommodates two kinds of Fe valence environments giving rise to a bimodal bond-distribution, with short and long Fe bonds. The bimodal bonds are present even as the system becomes superconducting in the presence of antiferromagnetism, with the weight continuously shifting from the short to the long with increasing K content. Such a hybrid state is most likely found in cuprates as well while our results point to the importance of the local atomic symmetry by which exchange interactions between local moments materialize.

Received
14 March 2013Accepted
6 June 2013Published
20 June 2013Correspondence and
requests for materials
should be addressed to
D.L. (louca@virginia.
edu)* Current address:
Basic Science College,
Daegu Gyeongbuk
Institute of Science and
Technology (DGIST),
Daegu 711-873,
Korea.

While suppression of long-range magnetic order has long been thought to be a pre-requisite to the onset of superconductivity, this rule is broken in the new class of iron-based superconductors^{1–4}, $K_xFe_{2-y}Se_2$, with T_c 's of the order of 30 K or so^{5,6}. Sandwiched between bad metallic ($x < \sim 0.7$) and insulating ($x > \sim 0.8$) antiferromagnetic states, it is found that superconductivity exists in tandem with antiferromagnetism, where the latter sets in at high temperatures, with T_N close to 560 K⁷. Even more peculiar is the size of the magnetic moment which is over $3\mu_B$ per Fe atom, a non-trivial quantity, and much larger than what is found in other pnictides and chalcogenides. Distinct to this system is the proposed presence of iron vacancies and of their ordering that gives rise to the $\sqrt{5} \times \sqrt{5} \times 1$ type ordered structure with the $I4/m$ crystal symmetry^{5,8–11}. Upon raising the temperature, it has been proposed that a vacancy order-disorder transition occurs at $T_S \sim 500$ K³, accompanied by a change of the crystal symmetry to $I4/mmm$. Are the vacancies ordered or disordered or even present in the superconducting state? It is currently argued that at the optimal x doping where superconductivity is found, phase separation occurs between the superconducting and non-superconducting regions of the sample, and that the superconducting component is stoichiometric with the KFe_2Se_2 composition (122 phase) and $I4/mmm$ symmetry that has no Fe vacancies⁷, while the insulating component has the $\sqrt{5} \times \sqrt{5} \times 1$ vacancy ordered structure. The Fe vacancies are considered destructive to superconductivity¹². What is the interplay among magnetism, superconductivity and vacancies, and do they microscopically coexist or are they phase separated? Here we show by probing the local atomic structure via neutron diffraction that the defect structure is not phase separated. Instead, a hybrid state is present with inhomogeneous potassium distribution that accommodates two types of Fe bonds that are tuned continuously by changing the composition and temperature.

Results

To identify the local symmetry that governs the Fe sublattice, two different crystal structure scenarios are considered. In the first scenario, the $I4/m$ symmetry of the vacancy ordered structure shown in Fig. 1(a) is assumed, where two distinct iron sites are present labeled Fe1 and Fe2 that give rise to three unique bond lengths due to Fe1-Fe1, Fe1-Fe2, and Fe2-Fe2 pair correlations. Details of the structure coordinates are provided in a supplemental table. The Fe1 site is the one that is partially occupied. In the second scenario, the $I4/mmm$ crystal symmetry is considered which is the symmetry found in the pnictides such as $Ba(Fe_{1-x}Co_x)_2As_2$ and only one unique Fe site is present^{13,14}. This symmetry does not hold any Fe vacancies and may be the symmetry appropriate for the superconducting phase in the proposed phase-separated scenario. To construct the local Fe environment expected from the two crystal symmetries, a real-space representation of the local structure is calculated from the atomic coordinates and unit cell dimensions of the two crystal structures¹⁵. The local model, presented in the form of the pair density function (PDF), $\rho(r)$, is a linear combination of all possible real-space atomic pair correlations,

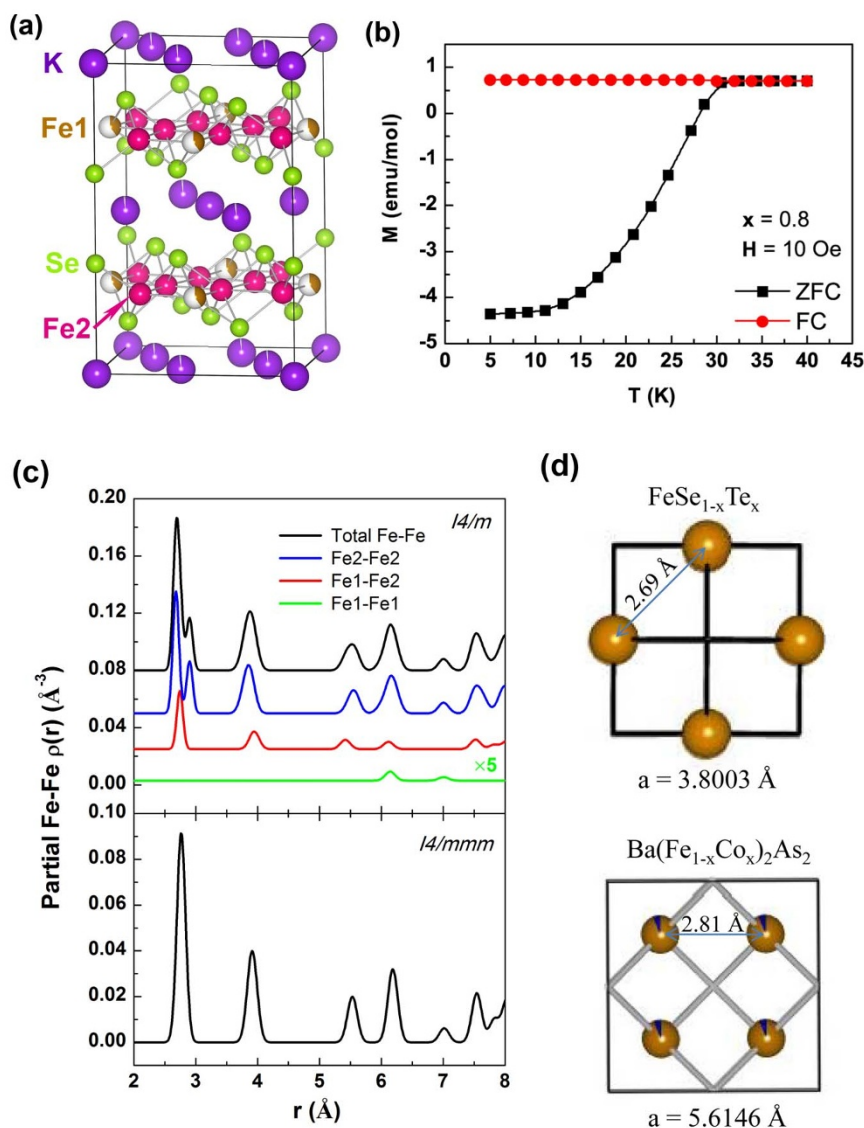


Figure 1 | Structure and magnetism. (a) The crystal structure of $K_xFe_{2-y}Se_2$ in the $I4/m$ symmetry with vacancies. (b) The temperature dependence of the magnetization from zero-field-cooled (ZFC) and field-cooled (FC) measurements at a magnetic field of 10 Oe for the $x = 0.8$. (c) (upper) In the $I4/m$ crystal structure, three kinds of Fe to Fe correlation functions are present based on the symmetry due to the two Fe positions. Also shown is the total Fe partial function in this symmetry. (lower) In the $I4/mmm$ crystal structure, only one kind of Fe to Fe correlation function is present. The parameters for the two crystal symmetries are provided in a supplemental Table. (d) Projecting on the ab -plane, only one Fe-Fe bond length is present in $FeSe_{1-x}Te_x$ (upper) and in $Ba(Fe_{1-x}Co_x)_2As_2$ (lower).

also known as partials. The partials corresponding to Fe to Fe correlations are shown in Fig. 1(c) where the x -axis is distance in real-space, r (\AA). The peaks correspond to the probability of finding a particular pair at the given distance. Given that the $I4/mmm$ symmetry hosts only one Fe site, only one Fe-Fe bond is seen at distances between 2.6–3 \AA (lower panel). Shown in the upper panels are the partial functions corresponding to Fe2-Fe2, Fe1-Fe2 and Fe1-Fe1 correlations calculated from the $I4/m$ symmetry. Since this symmetry holds two Fe sites, the combined total partial function for Fe has two peaks at distances in the range of 2.6–3 \AA . Note that no other pairs contribute to this region of space. For comparison, shown in Fig. 1(d) are plots of the Fe-Fe square plaquettes in two other Fe-based superconducting systems where a single Fe-Fe bond length is present: in $FeSe_{1-x}Te_x$ ¹⁵ with a length at 2.69 \AA (in the $P4/nmm$ symmetry) and in $Ba(Fe_{1-x}Co_x)_2As_2$ ^{14,16} with a length at 2.81 \AA (in the $I4/mmm$ symmetry). Of the two possible local Fe environments, the one present in $K_xFe_{2-y}Se_2$ will be decided upon comparing the local models to the local structure obtained from the neutron diffraction data.

Details of this technique can be found in Ref. 17. From the experiment, we obtain the total PDF and not the individual partials.

Three chemical compositions, corresponding to three regions of the phase diagram as defined in Ref. 7, were measured in order to study the evolution of the local atomic structure: one in region I (high Fe valence) at $x = 0.6$, one in region II (intermediate Fe valence) at $x = 0.8$, and a third one in region III (low Fe valence) at $x = 1.0$. Only one of these samples is superconducting, the $x = 0.8$, with a T_C of about 30 K. Its bulk susceptibility is shown in Fig. 1(b). The experimentally determined $\rho(r)$ is obtained by a Fourier transform of the total structure function, the latter reaching out to high momentum transfers (42\AA^{-1}). Shown in Fig. 2(a) is the $\rho(r)$ corresponding to the local structure for the three compositions at 2 K while in 2(b), the data for the same compositions were collected at 200 K. As the potassium concentration increases, the function shifts to the right because the lattice expands in addition to changing shape. How is the shape change accounted for? As seen in the figures, in the region where the Fe-Fe bonds are expected, two peaks are present and



indicated by arrows albeit with different weights. The presence of two Fe-Fe correlations closely resembles what is expected from the $I4/m$ symmetry (see Fig. 1(c)) and not from the $I4/mmm$. As x increases from 0.6 to 1.0, the weight distribution under the short (peak to the left ~ 2.68 Å) and long (peak to the right ~ 2.87 Å) Fe-Fe bond lengths continuously shifts from the short to the long while the position of the peaks does not. Most clearly is the presence of both short and long Fe-Fe bonds in the superconducting composition, right in-between the other two compositions. At 200 K in Fig. 2(b), a redistribution of the weight under the short Fe-Fe peak is observed as it shifts to the longer length with the intensity of the peak rising with increasing x . Focusing on the temperature dependence of the local structure of the $x = 0.8$ superconductor alone, in Fig. 2(c), it can be seen that the width of the short Fe-Fe peak increases as its height decreases with increasing temperature, the latter shown in the inset of this figure with red symbols. The second long Fe-Fe bond peak gains a bit in height (see inset with blue symbols) as it slightly shifts to the left. Back to the composition dependence at 2 K, the region under the two Fe-Fe peaks is fit by two Gaussians, and the integrated area, which is proportional to the local coordination number, is shown for each composition in Figs. 2(d)–(f). The continuous shift from the short to the long bonds as a function of x is evident here as well, but at all times, both peaks are present. The higher ratio of short to long bonds in $x = 0.6$ indicates

that there are more short Fe-Fe neighbors than long in this composition. This is followed by an equal ratio of short to long Fe-Fe bonds in $x = 0.8$. And finally, in the $x = 1.0$, there are more long Fe-Fe bonds than short. This serves as evidence for a continuous structural evolution with doping.

Discussion

How can we describe the local microstructure of the superconducting state? The double-well Fe bond distribution in the $x = 0.8$ superconductor can be well explained by a linear combination of the data sets for the $x = 0.6$ (region I) and $x = 1.0$ (region III) doped materials. This is shown in Fig. 3(a), and involves no rescaling of the PDF's. This demonstrates that the bimodal Fe bond distribution in the Fe plaquette of the superconducting $x = 0.8$ is consistent with there being regions in the structure closely resembling the $x = 0.6$ and $x = 1.0$ Fe plaquettes, implying an inhomogeneous K distribution¹⁸. The superposition of the local structures for $x = 0.6$ and 1.0 also implies that the structure evolves continuously by doping K into the vacancy ordered $\sqrt{5} \times \sqrt{5} \times 1$ phase. The 1:1 ratio demonstrates that the bimodal Fe-Fe distribution in the $x = 0.8$ data is consistent with there being two valence states of Fe. The valence state of Fe has a direct effect on the Fe-Fe bond length. The double-well Fe-Fe distribution of Figs. 2(d–f) indicates that two Fe valence environments are present at all times. The shift to the longer length with x indicates that

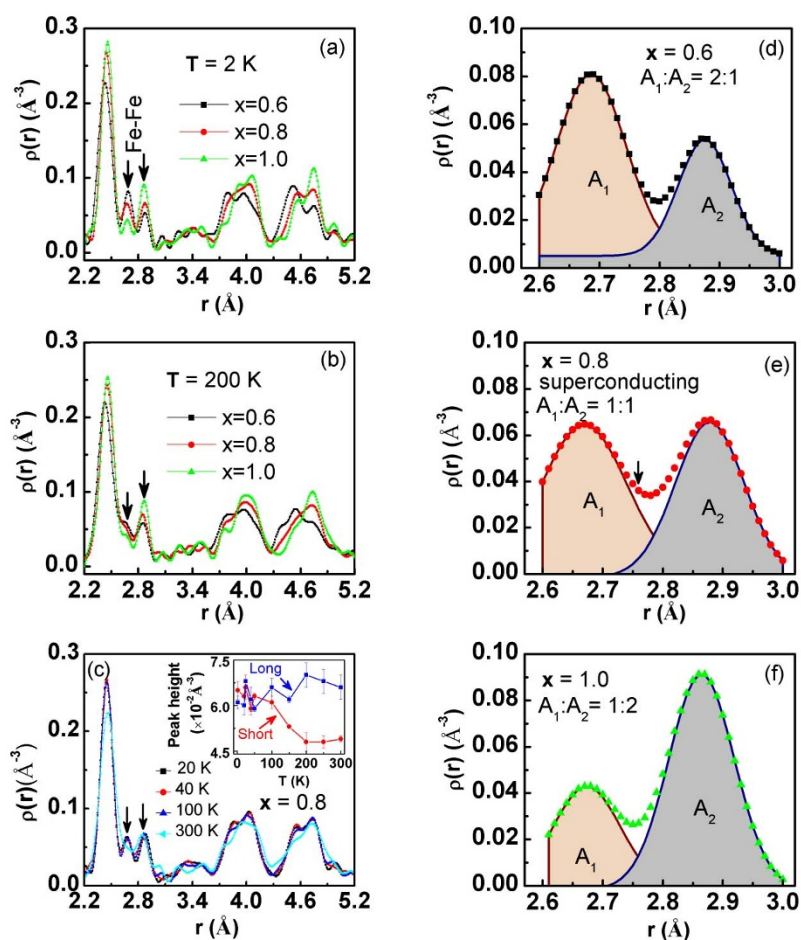


Figure 2 | Experimental local structure. The pair density function is determined from the neutron data collected from the $x = 0.6, 0.8$ and 1.0 crystals at 2 K in (a) and 200 K in (b). Differences are observed across real space, especially in the region from 2.6 to 3.0 Å where two Fe to Fe correlations (long and short) are present. (c) The temperature dependence of the local structure corresponding to the superconducting $x = 0.8$. The width of the short Fe-Fe peak broadens with increasing temperature due to an increase in the short Fe-Fe bond distribution. In the inset, the peak height for the short (red) and long (blue) Fe-Fe bonds are plotted. The error bars are one standard deviation. (d)–(f) In the region from 2.6 to 3.0 Å of the $\rho(r)$, the short and long Fe-Fe peaks are fit by two Gaussians functions. The ratio of the integrated intensity corresponding to the long and short Fe bonds is shown in each panel. Marked on (e) with an arrow is the possible position of the Fe-Fe peak had the $I4/mmm$ symmetry been present.



the valence of Fe goes down while the shift to the shorter length indicates that the Fe valence goes up. It was previously noted that the Seebeck coefficient changes systematically with the Fe valence that corresponds to a change in the type of charge carriers⁷. The superconducting composition shows both Fe environments and also a very small Seebeck coefficient, leading to a Lifshitz transition¹⁹.

Which symmetry can best describe the local structure of the superconducting sample? If we were to assume a 100 % volume fraction of the $I4/mmm$ symmetry, such a model would generate an intermediate Fe-Fe peak (Fig. 3(b) – orange line) that resides in between the experimentally observed short and long Fe peaks and is clearly not present. If we were to assume a 100 % volume fraction of the $I4/m$ symmetry taking into account the partial occupancy of the Fe1 site, such a model would generate the peaks at the right positions also shown in Fig. 3(b). However, even though the $\sqrt{5} \times \sqrt{5} \times 1$ structure yields two Fe-Fe peaks, their intensity ratio does not correspond to the equally distributed double-well Fe bonds observed experimentally in the $x = 0.8$ data set because this model does not consider the local potassium inhomogeneity mentioned earlier, which in turn has an effect on the Fe environment. A mixed $I4/m$ with $I4/mmm$ at 50 % volume fraction yields a model PDF shown as the blue line in this figure. The addition of $I4/mmm$ takes the weight away from the long Fe-Fe bonds and shifts the short Fe-Fe bonds to the right, hence such

a volume fraction ratio is not appropriate. It is clear that the addition of any amount of $I4/mmm$ will lead to a shift of the bonds. At the same time, if the $I4/mmm$ volume fraction is less than 10 %, the changes in the local structure are not easily discerned. However the superconducting volume fraction was estimated to be about 80 % at 5 K, which is contradictory to possibly only having 10 % or less volume fraction of the presumed $I4/mmm$ symmetry of the superconducting phase.

Locally, to create a bimodal Fe valence environment and reproduce the experimental configuration observed in the $x = 0.8$, it is necessary to expand the inner square made of Fe2 (red atoms) in the plaquette as shown in Figs. 3(c) corresponding to the $x = 0.6$ structure towards the one of Fig. 3(d) which corresponds to the $x = 1.0$ structure. In the crystal symmetry of the $I4/m$, the number of Fe2-Fe2 bonds is the majority at ~ 2.68 Å while the number of the longer Fe2-Fe2 bonds at ~ 2.87 Å bonds is the minority. The bonds between Fe1-Fe2 contribute little to the overall count because of the low concentration of Fe1. Thus to increase the number of bonds with the longer lengths, it requires that a fraction of the inner Fe2 atoms—marked by a green square in the plaquette expand from the configuration shown in Fig. 3(c) to the configuration shown in Fig. 3(d). Such a local distortion will initially appear in some parts of the sample, but as the concentration of K increases, it spreads to more

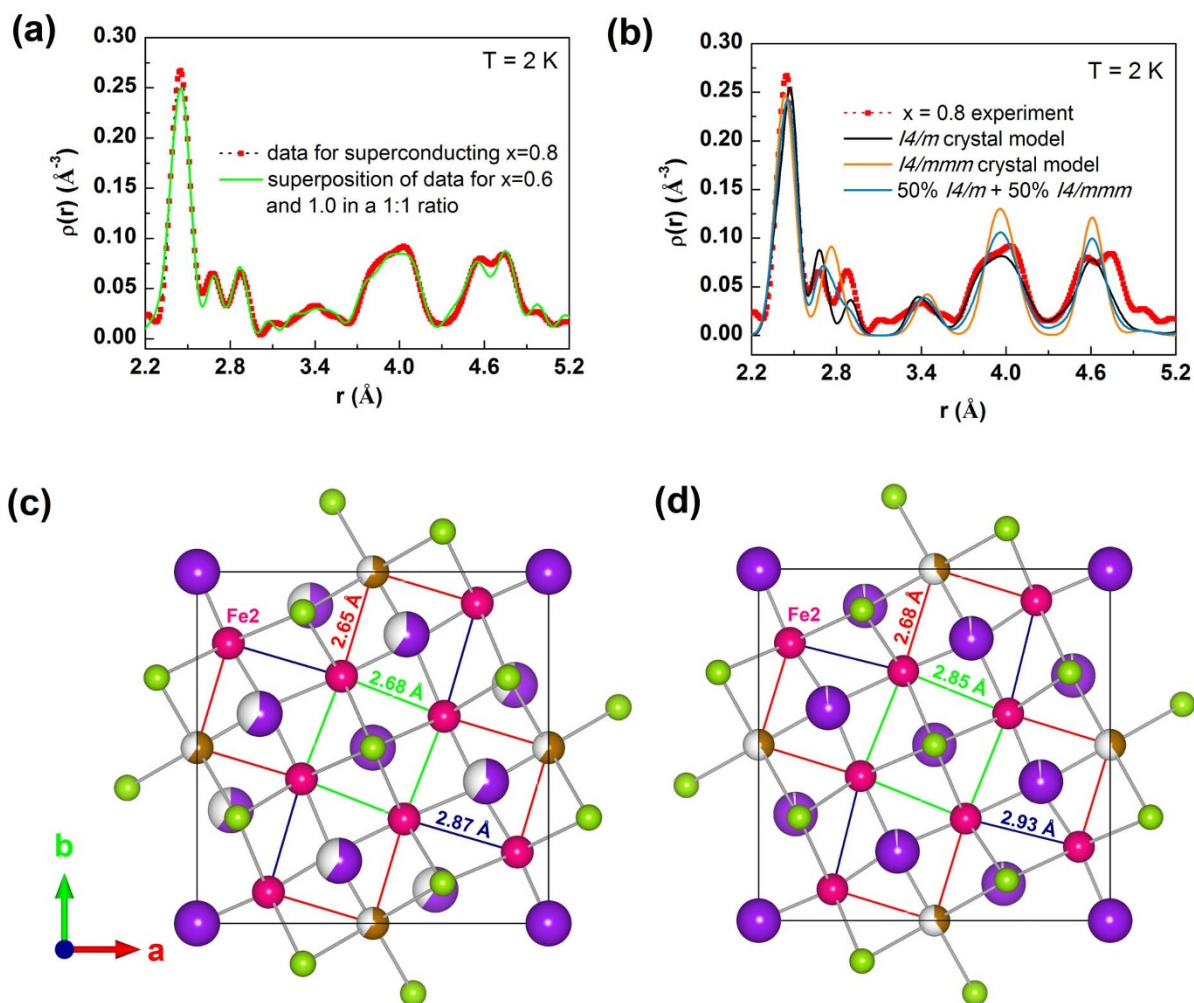


Figure 3 | Local structure environment. (a) The experimentally determined pair density function for the $x = 0.8$ is compared to a linear superposition of the structures corresponding to the $x = 0.6$ and 1.0 at 2 K. (b) The pair density function for the $x = 0.8$ is compared to three models, calculated using the parameters of the $I4/m$ and the $I4/mmm$ crystal symmetries. (c) and (d) are projections on the ab -plane showing the Fe-Fe bonds for the $x = 0.6$ (c) and for the $x = 1.0$ (d) compositions. The superconducting phase is a hybrid of the two. From the $x = 0.6$ to the $x = 1.0$ structure, the inner Fe2 square lattice expands, reducing the number of short bonds while increasing the number of long Fe bonds.



sites, hence the shift to longer bonds. An analogous shift occurs as the temperature rises above T_C (Fig. 2(c)), where the number of short bonds goes down even though the concentration of K does not change and the ions cannot diffuse at such low temperatures. This indicates that the bimodal Fe-Fe distribution is very sensitive to temperature as well and is possibly crucial to superconductivity. What determines the critical concentration of $x = 0.8$ may well rest in this local arrangement that in turn leads to changes of the Fermi surface. Having such an inhomogeneous environment may be conducive to a complex ground state where two order parameters are viable. This may be more frequent in nature than previously anticipated as recent reports of a charge-density wave order in the superconducting state of $\text{YBa}_2\text{Cu}_3\text{O}_{6+y}$ are revealing^{20–22}.

In other Fe-based superconductors, it has been shown that the Fermi surface consists of hole and electron pockets while nesting may lead to a spin density wave²³. However, $\text{K}_x\text{Fe}_{2-y}\text{Se}_2$ is devoid of hole pockets at the zone center where strong antiferromagnetic ordering is present that cannot be explained by nesting^{24–27}. From the structure point of view, this system is distinctly different from the $\text{FeSe}_x\text{Te}_{1-x}$ class with T_C 's ranging from 8–14 K, where only one distribution of Fe-Fe bond length is observed. Similarly, in the pnictide $\text{Ba}(\text{Fe}_{1-x}\text{Co}_x)_2\text{As}_2$ only a single Fe-Fe bond type is observed also. While in both of these systems, no static long-range AFM order exists, this is in contrast to the K system, where all samples exhibit static antiferromagnetic order. The presence of local disorder lowers the lattice symmetry that must in turn influence the electron-phonon interactions and T_C ^{28–31}. It is conceivable that such a disorder would weaken the coupling constant leading to a change in the electron and phonon density of states.

Methods

The $\text{K}_x\text{Fe}_{2-y}\text{Se}_2$ single crystals used in this study were grown by a modified Bridgman technique. The FeSe precursor, prepared separately, was mixed with pieces of K metal. The mixture was sealed in a glass tube in a glove box under Ar atmosphere and heated up to 1030 °C for 12 hours. After 4 hours held at that temperature, the sample was cooled down to 730 °C at 5 K/min and then quenched in air by turning off the power to the furnace. Three nominal compositions were prepared: $\text{K}_{0.6}\text{Fe}_{2-y}\text{Se}_2$, $\text{K}_{0.8}\text{Fe}_{2-y}\text{Se}_2$ and $\text{KFe}_{2-y}\text{Se}_2$. The concentration of Fe was refined to be 1.624 for $\text{K} = 0.6$, 1.632 for $\text{K} = 0.8$, and 1.76 for $\text{K} = 1$. The bulk magnetic susceptibility measurements from 5 to 50 K showed that $T_C \sim 30$ K for the $\text{K}_{0.8}\text{Fe}_{2-y}\text{Se}_2$ crystals only, while no superconductivity was observed for the other two compositions. The neutron experiments were carried out using the NOMAD diffractometer at the Spallation Neutron Source of Oak Ridge National Laboratory as a function of temperature, from 2 to 300 K. The single crystals were ground into powder inside a dry glove box prior to the experiment and held in an evacuated vanadium can in a duplex refrigeration system.

- Kamihara, Y., Watanabe, T., Hirano, M. & Hosono, H. Iron-based layered superconductor $\text{La}[\text{O}_{1-x}\text{F}_x]\text{FeAs}$ ($x = 0.05\text{--}0.12$) with $T_c = 26$ K. *J. Am. Chem. Soc.* **130**, 3296–3297 (2008).
- Rotter, M., Tegel, M. & Johrendt, D. Superconductivity at 38 K in the iron arsenide $(\text{Ba}_{1-x}\text{K}_x)\text{Fe}_2\text{As}_2$. *Phys. Rev. Lett.* **101**, 107006 (2008).
- Bao, W. *et al.* Vacancy tuned magnetic high- T_C superconductor $\text{K}_x\text{Fe}_{2-x/2}\text{Se}_2$. *Chinese Phys. Lett.* **30**, 027402 (2013).
- Guo, J. G. *et al.* Superconductivity in the iron selenide $\text{K}_x\text{Fe}_2\text{Se}_2$ ($0 \leq x \leq 1.0$). *Phys. Rev. B* **82**, 180520(R) (2010).
- Bao, W. *et al.* A novel large moment antiferromagnetic order in $\text{K}_{0.8}\text{Fe}_{1.6}\text{Se}_2$ superconductor. *Chin. Phys. Lett.* **28**, 086104 (2011).
- Wang, M. Y. *et al.* Spin waves and magnetic exchange interactions in insulating $\text{Rb}_{0.89}\text{Fe}_{1.58}\text{Se}_2$. *Nature Commun.* **2**, 580 (2011).
- Yan, Y. J. *et al.* Electronic and magnetic phase diagram in $\text{K}_x\text{Fe}_{2-y}\text{Se}_2$ superconductors. *Nature Scientific Reports* **2**, 00212 (2012).
- Ye, F. *et al.* Common crystalline and magnetic structure of superconducting $\text{A}_2\text{Fe}_4\text{Se}_5$ ($\text{A} = \text{K}, \text{Rb}, \text{Cs}, \text{Tl}$) single crystals measured using neutron diffraction. *Phys. Rev. Lett.* **107**, 137003 (2011).
- Fang, M.-H. *et al.* Fe-based superconductivity with $T_c = 31$ K bordering an antiferromagnetic insulator in $(\text{Tl}, \text{K})\text{Fe}_x\text{Se}_2$. *Europhys. Lett.* **94**, 27009 (2011).
- Wang, Z. *et al.* Microstructure and ordering of iron vacancies in the superconductor system $\text{K}_x\text{Fe}_x\text{Se}_2$ as seen via transmission electron microscopy. *Phys. Rev. B* **83**, 140505(R) (2011).

- Ricci, A. *et al.* Nanoscale phase separation in the iron chalcogenides superconductor $\text{K}_{0.8}\text{Fe}_{1.6}\text{Se}_2$ as seen via scanning nanofocused x-ray diffraction. *Phys. Rev. B* **84**, 060511 (2011).
- Li, W. *et al.* Phase separation and magnetic order in K-doped iron selenide superconductor. *Nature Phys.* **8**, 126 (2012).
- Park, K., Louca, D., Llobet, A. & Yan, J.-Q. Evidence of local disorder in the overdoped regime of $\text{Ba}(\text{Fe}_{1-x}\text{Co}_x)_2\text{As}_2$. *Phys. Rev. B* **84**, 024512 (2011).
- Huang, Q. *et al.* Neutron-diffraction measurements of magnetic order and a structural transition in the parent BaFe_2As_2 compound of FeAs-based high-temperature superconductors. *Phys. Rev. Lett.* **101**, 257003 (2008).
- Louca, D. *et al.* Local atomic structure of superconducting $\text{FeSe}_{1-x}\text{Te}_x$. *Phys. Rev. B* **81**, 134524 (2010).
- Ni, N. *et al.* Effects of Co substitution on thermodynamic and transport properties and anisotropic H_{c2} in $\text{Ba}(\text{Fe}_{1-x}\text{Co}_x)_2\text{As}_2$ single crystals. *Phys. Rev. B* **78**, 214515 (2008).
- Egami, T. & Billinge, S. J. L. *Underneath the Bragg Peaks: Structural Analysis of Complex Materials* (Pergamon, Materials Series, Vol. 7, 2003).
- Lei, H. & Petrovic, C. Anisotropy in transport and magnetic properties of $\text{K}_{0.64}\text{Fe}_{1.44}\text{Se}_2$. *Phys. Rev. B* **83**, 184504 (2011).
- Liu, C. *et al.* Evidence of a Lifshitz transition in electron-doped iron arsenic superconductors at the onset of superconductivity. *Nature Phys.* **6**, 419–423 (2010).
- Frarkin, E. & Kivelson, S. A. High-temperature superconductivity: ineluctable complexity. *Nature Phys.* **8**, 864 (2012).
- Chang, J. *et al.* Direct observation of competition between superconductivity and charge density wave order in $\text{YBa}_2\text{Cu}_3\text{O}_{6.67}$. *Nature Phys.* **8**, 871 (2012).
- Ghiringhelli, G. *et al.* Long-Range Incommensurate Charge Fluctuations in $(\text{Y}, \text{Nd})\text{Ba}_2\text{Cu}_3\text{O}_{6+x}$. *Science* **337**, 821 (2012).
- Chen, H. *et al.* Coexistence of the spin-density wave and superconductivity in $\text{Ba}_{1-x}\text{K}_x\text{Fe}_2\text{As}_2$. *Europhys. Lett.* **85**, 17006 (2009).
- Arita, R. & Ikeda, H. Is Fermi-surface nesting the origin of superconductivity in iron pnictides? A fluctuation-exchange-approximation study. *J. Phys. Soc. Jpn* **78**, 113707 (2009).
- Qian, T. *et al.* Absence of holelike Fermi surface in superconducting $\text{K}_{0.8}\text{Fe}_{1.7}\text{Se}_2$ revealed by ARPES. *Phys. Rev. Lett.* **106**, 187001 (2011).
- Wang, X.-P. *et al.* Strong nodeless pairing on separate electron Fermi surface sheets in $(\text{Tl}, \text{K})\text{Fe}_{1.78}\text{Se}_2$ probed by ARPES. *Europhys. Lett.* **93**, 57001 (2011).
- Mou, D. *et al.* Distinct Fermi surface topology and nodeless superconducting gap in a $(\text{Tl}_{0.58}\text{Rb}_{0.42})\text{Fe}_{1.72}\text{Se}_2$ superconductor. *Phys. Rev. Lett.* **106**, 107001 (2011).
- Panova, G. K., Chernoplekov, N. A., Shikov, A. A. & Savel'ev, B. I. Changes in the superconducting properties of the $\text{Zr}_{75}\text{Rh}_{25}$ system on becoming amorphous. *Sov. Phys. JETP* **55**(2), 319 (1982).
- Johnson, J. L., Poon, S. J. & Duwez, P. Amorphous superconducting lanthanum-gold alloys obtained by liquid quenching. *Phys. Rev. B* **11**, 150 (1975), and references therein.
- Jorgensen, J. D. Defects and superconductivity in the copper oxides. *Physics Today* **44**(6), 34–40 (1991).
- Kotliar, G. & Kapitulnik, K. Anderson localization and the theory of dirty superconductors II. *Phys. Rev. B* **33**, 3146 (1986).

Acknowledgements

The work at the University of Virginia has been supported by the U. S. Department of Energy, Office of Basic Energy Sciences, under contract number DE-FG02-01ER45927.

Author contributions

Single crystals of $\text{K}_x\text{Fe}_{2-y}\text{Se}_2$ were grown by K.P. The magnetic susceptibility measurements were carried out by J.Y. and K.P. K.P., D.L. and J.N. carried out the neutron measurements. D.L. wrote the main manuscript text, carried out the analysis and prepared the figures with B.L., D.L. was responsible for project direction, planning and infrastructure. All authors reviewed the manuscript.

Additional information

Supplementary information accompanies this paper at <http://www.nature.com/scientificreports>

Competing financial interests: The authors declare no competing financial interests.

How to cite this article: Louca, D., Park, K., Li, B., Neufeld, J. & Yan, J.Q. The hybrid lattice of $\text{K}_x\text{Fe}_{2-y}\text{Se}_2$: where superconductivity and magnetism coexist. *Sci. Rep.* **3**, 2047; DOI:10.1038/srep02047 (2013).



This work is licensed under a Creative Commons Attribution-NonCommercial-NoDerivs 3.0 Unported license. To view a copy of this license, visit <http://creativecommons.org/licenses/by-nc-nd/3.0>